

The Isoline Tracking in Unknown Scalar Fields with Concentration Feedback

Fei Dong, Keyou You *

Department of Automation and BNRist, Tsinghua University, Beijing 100084, China.

Abstract

The isoline tracking of this work is concerned with the control design for a sensing vehicle to track a desired isoline of an unknown scalar field. To this end, we propose a simple PI-like controller for a Dubins vehicle in the GPS-denied environments. Our key idea lies in the design of a novel sliding surface based error in the standard PI controller. For the circular field, we show that the P-like controller can *globally* regulate the vehicle to the desired isoline with the steady-state error that can be arbitrarily reduced by increasing the P gain, and is eliminated by the PI-like controller. For any smoothing field, the P-like controller is able to achieve the local regulation. Then, it is extended to the cases of a single-integrator vehicle and a double-integrator vehicle, respectively. Finally, the effectiveness and advantages of our approaches are validated via simulations on the fixed-wing UAV and quadrotor simulators.

Key words: Scalar field, isoline tracking, PI-like controller, regulation.

1 Introduction

The isoline tracking commonly refers to the tactic that a sensing vehicle reaches and then tracks a desired concentration level of a scalar field with unknown distribution, which has wide applications in the environmental exploration, e.g., tracking curve of sea temperature (Zhang & Leonard 2010), tracking boundary of volcanic ash (Kim et al. 2017), tracking plume front of oil spill (Jiang & Li 2018), exploring environmental feature of bathymetric depth (Mellucci et al. 2019), and monitoring algal bloom (Fonseca et al. 2019). In the literature, it is also named as level set tracking (Matveev et al. 2012), curve tracking (Malisoff et al. 2017), boundary tracking (Menon et al. 2015, Matveev et al. 2017, Kim et al. 2017, Mellucci et al. 2019), and covers the celebrated target circumnavigation as a special case (Matveev et al. 2011, Deghat et al. 2012, Cao 2015, Swartling et al. 2014, Zheng et al. 2015, Dong, You & Xie 2020, López-Nicolás et al. 2020, Dong, You & Song 2020).

Compared with the static sensor networks, it is more flexible and economical to utilize sensing vehicles to col-

lect data or track targets. Roughly speaking, we can categorize the control methods for the isoline tracking depending on whether the gradient of the scalar field can be used or not. The gradient-based method is extensively used to steer a vehicle to track the direction of gradient descending (ascending) to the minimizer (maximizer) of a scalar field (Zhang & Leonard 2010, Briñón-Arranz et al. 2019, Bourne et al. 2019). This strategy can also be extended to the problem of the isoline tracking (Kapitanyuk et al. 2018).

If the gradient is not explicitly available, many works focus on the gradient estimation problem (Briñón-Arranz et al. 2019, Hwang et al. 2019), including that (a) one vehicle changes its position over time to collect the signal propagation at different locations; and (b) multiple vehicles collaborate to obtain measurements at different locations at the same time. For example, Ai et al. (2016) design a sequential least-squares field estimation algorithm for a REMUS AUV to seek the source of a hydrothermal plume. The stochastic method for extreme seeking is gradient-based in nature, the idea behind which is to approximate the gradient of the field by adding an excitatory input to the controller (Cochran et al. 2009, Lin et al. 2017, Li et al. 2020). In Briñón-Arranz et al. (2019), a circular formation of vehicles is adopted to estimate the gradient of the sensing field. Moreover, both cooperative Kalman filter and \mathcal{H}_∞ filter are devised to estimate the gradient in Zhang & Leonard

* This work was supported in part by the National Natural Science Foundation of China under Grant 61722308.

* Corresponding author

Email addresses: dongf17@mails.tsinghua.edu.cn (Fei Dong), youky@tsinghua.edu.cn (Keyou You).

(2010) and Wu & Zhang (2012), respectively. A particle filter has been developed to estimate a Gaussian plume model where multiple vehicles are coordinated via the multimodal nature of the nonparametric posterior in Bourne et al. (2019).

However, in many practical scenarios, the vehicles have no access to its GPS position and can only obtain the concentration measurement at the current location, i.e., the measurement is in a point-wise fashion (Matveev et al. 2012). Thus, it is of interest to exploit gradient-free methods without position information. A sliding mode approach has been proposed for the target circumnavigation in Matveev et al. (2011) and then adopted to the level set tracking (Matveev et al. 2012), boundary tracking (Matveev et al. 2015), and etc. They address the “chattering” phenomenon via modeling dynamics of the actuator as a first-order linear differential equation. However, there is no rigorous proof of the revised control law. A PD feedback controller is devised in Baronov & Baillieul (2007) for a double-integrator vehicle to follow isolines in a harmonic potential field. A PID controller with adaptive crossing angle correction is designed in Newaz et al. (2018). Moreover, there are some heuristic methods for the isoline tracking, e.g., the sliding mode control (Menon et al. 2015, Mellucci et al. 2017), the bang-bang type control (Joshi et al. 2009), and etc. The sliding mode controller consists of two-sliding motions to explore the environmental feature of bathymetric depth. They validate their controller via simulations in a synthetic data-based environment and sea-trials via a C-Enduro ASV. The bang-bang type control switches between alternative steering angles in virtue of whether the current measurement is above or below the threshold of interest, which results in a zigzagging behavior.

In this paper, we propose a gradient-free controller in a PI-like form for a Dubins vehicle to track a desired isoline by using only the concentration feedback. That is, we do not use any field gradient or the position of the sensing vehicle, which is particularly useful in GPS-denied environments. Our key idea lies in the design of a novel sliding surface based error in the standard PI controller. Then we show that the steady-state tracking error can be reduced by simply increasing the P gain, and is eliminated for circular fields with a small I gain. For the case of smoothing scalar fields, we explicitly show the upper bound of the steady-state tracking error, which also can be reduced by increasing the P gain. To validate the effectiveness of our PI-like controller via simulation, we adopt a fixed-wing UAV to track the predefined isoline of the concentration distribution of particulate matter (PM2.5) based on a real dataset in an area of China. Finally, we extend the PI-like controller to the cases of a single-integrator vehicle and a double-integrator vehicle, respectively. A preliminary version of this work which only considers the case of a Dubins vehicle is presented in Dong & You (2020).

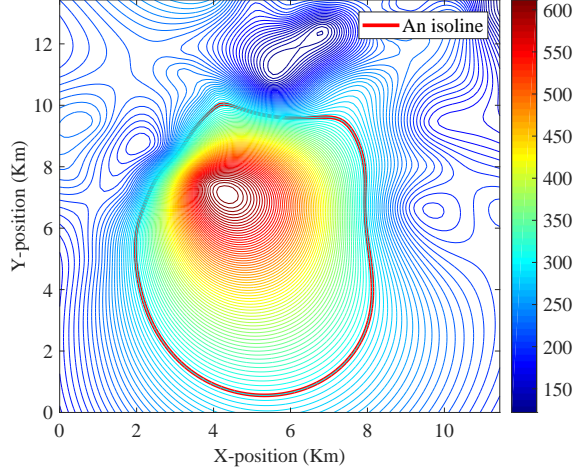


Fig. 1. The PM2.5 concentration observed in an area of China.

The rest of this paper is organized as follows. In Section 2, we explicitly describe the isoline tracking problem. To solve it, we propose a simple PI-like controller in Section 3. In Section 4, we show the global convergence and local exponential stability for the case of circular fields. In Section 5, we study the closed-loop stability of the PI-like controller in a smoothing scalar field. The extension to the cases of a single-integrator vehicle and a double-integrator vehicle are given in Section 6. Finally, simulations are performed in Section 7, and some concluding remarks are drawn in Section 8.

2 Problem Formulation

In Fig. 1, we provide a 2-D example of the concentration distribution of PM2.5 based on a real dataset in an area of China¹. To monitor the environment, it is fundamentally important to investigate the spatial distribution of PM2.5. That is, we design a sensing vehicle to track an isoline of its distribution function, which is described as

$$F(\mathbf{p}) : \mathbb{R}^2 \rightarrow \mathbb{R}, \quad (1)$$

where $\mathbf{p} \in \mathbb{R}^2$ is a GPS position in 2-D. Given a concentration level s_d , an isoline $\mathcal{L}(s_d)$ of $F(\mathbf{p})$ is defined as

$$\mathcal{L}(s_d) = \{\mathbf{p} | F(\mathbf{p}) = s_d\}. \quad (2)$$

The *isoline tracking* problem is on the control design for a sensing vehicle to move along with the desired isoline $\mathcal{L}(s_d)$. Precisely, the position $\mathbf{p}(t)$ of the sensing vehicle is controlled to satisfy that

$$\lim_{t \rightarrow \infty} |s(t) - s_d| \rightarrow 0 \text{ and } \|\dot{\mathbf{p}}(t)\| = v, \quad (3)$$

¹ For privacy concern, we do not provide the exact region of the collected data.

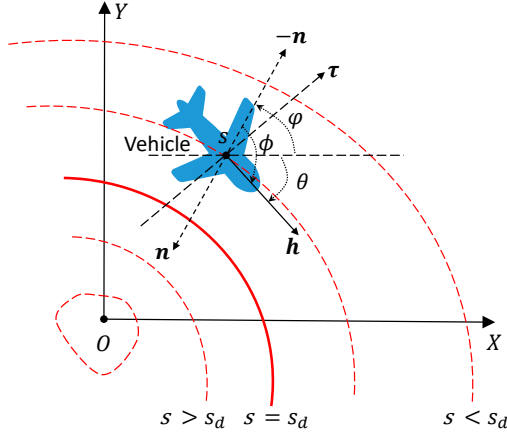


Fig. 2. Coordinates of the Dubins vehicle in scalar fields.

where $s(t) = F(\mathbf{p}(t))$ is the concentration of the scalar field at the position $\mathbf{p}(t)$ and v denotes a constant linear speed of the vehicle. Throughout this work, we always focus on the following scenario.

- (a) Neither the concentration distribution function $F(\cdot)$ nor the GPS position of the vehicle $\mathbf{p}(t)$ is known.
- (b) We cannot measure a continuum of the scalar field, and the vehicle can only obtain $s(t)$ at its current position $\mathbf{p}(t)$.
- (c) s_d is not an extreme point of $F(\cdot)$.

The above implies that the gradient-based methods in Zhang & Leonard (2010), Malisoff et al. (2017), Kapitanyuk et al. (2018), Briñón-Arranz et al. (2019) cannot be applied. If s_d is an extreme point of $F(\cdot)$, the isoline may be degenerated into a single point or a set with positive Lebesgue measure, in which case the isoline tracking problem is not well defined in this work.

3 Controller Design for Dubins Vehicles

In this section, we design a gradient-free controller in a PI-like form for a Dubins vehicle to complete the isoline tracking task. Our key idea lies in the design of a novel sliding surface based error in the standard PI controller. The cases of a single-integrator vehicle and a double-integrator vehicle are given in Section 6.

Consider a Dubins vehicle on a 2-D plane

$$\dot{\mathbf{p}}(t) = v \begin{bmatrix} \cos \theta(t) \\ \sin \theta(t) \end{bmatrix} \text{ and } \dot{\theta}(t) = \omega(t), \quad (4)$$

where $\mathbf{p}(t) \in \mathbb{R}^2$, $\theta(t)$, $\omega(t)$ and v denote the GPS position, heading course, tunable angular speed and constant linear speed, respectively. See Fig. 2 for illustration.

To achieve the tracking objective in (3) by the Dubins vehicle, we propose the following PI-like controller

$$\omega(t) = c_1 e(t) + c_2 \sigma(t), \quad (5)$$

where $\sigma(t) = \int_0^t e(\tau) d\tau$ is an integrator, $e(t)$ is the output of a nonlinear system driven by the tracking error $\varepsilon(t) = s(t) - s_d$, and $c_{1,2} \geq 0$ are the control parameters to be designed.

The major difference of (5) from the PI controller lies in the novel design of the following error system

$$e(t) = \dot{\varepsilon}(t) + c_3 \tanh(\varepsilon(t)/c_4), \quad (6)$$

where $c_{3,4} > 0$ are constant parameters and $\tanh(\cdot)$ is the standard hyperbolic tangent function. In fact, $e(t) = 0$ also can be regarded as a sliding surface. If the surface is maintained, i.e.,

$$\dot{\varepsilon}(t) = -c_3 \tanh(\varepsilon(t)/c_4), \quad (7)$$

then $\varepsilon(t)$ will tend to zero with an exponential convergence speed.

If we directly set $c_2 = 0$, then (5) is reduced to a P-like controller

$$\omega(t) = c_1 e(t). \quad (8)$$

Note that the P-like controller in (5) is designed for the global stability, and the I-like controller is added to eliminate the steady-state error. Similar to the standard PI controller, it typically requires that $0 \leq c_2 \ll c_1$. In view of (7), c_3 affects the convergence speed and c_4 affects the sensitivity to the tracking error $\varepsilon(t)$.

Since the PI-like controller (5) only uses the tracking error $\varepsilon(t)$ and its derivative $\dot{\varepsilon}(t)$, it is particularly useful in the GPS-denied environments.

Remark 1 *If $\dot{\varepsilon}(t)$ is unavailable, we can design a second order sliding mode (SOSM) filter (Dong, You & Xie 2020), a first order filter (Guler & Fidan 2015), or a washout filter (Lin et al. 2016) to address this issue, which is not pursued in this work.*

4 The Isoline Tracking in Circular Fields

In this section, we consider a simplified yet instructive case of a circular field, which includes the acoustic field, i.e.,

$$F(\mathbf{p}) = I_0 \exp(-\alpha \|\mathbf{p} - \mathbf{p}_o\|_2), \quad (9)$$

where \mathbf{p}_o is the source position of the field and I_0, α are unknown positive parameters. Taking logarithmic functions on both sides of (9), then $\ln(F(\mathbf{p})) = \ln I_0 -$

$\alpha\|\mathbf{p}(t) - \mathbf{p}_o\|_2$. From the mathematical proof of view, there is no loss of generality to directly write the concentration function of a circular field as

$$F(\mathbf{p}) = s_d - \alpha(r(t) - r_d), \quad (10)$$

where $r(t) = \|\mathbf{p} - \mathbf{p}_o\|_2$ is the distance from the vehicle to the source position, and r_d is unknown. Clearly, $F(\mathbf{p}) = s_d$ if and only if $r(t) = r_d$, and r_d is desired distance for the vehicle to maintain from the source position \mathbf{p}_o .

By Fig. 2, let $\mathbf{n} = \nabla F(\mathbf{p})$ denote the gradient of $F(\mathbf{p})$ at the position \mathbf{p} , $\mathbf{h} = [\cos \theta, \sin \theta]'$ represent the heading vector of the vehicle, and $\boldsymbol{\tau}$ be a tangent vector of \mathbf{h} . By convention, \mathbf{h} and $\boldsymbol{\tau}$ form a right-handed coordinate frame with $\mathbf{h} \times \boldsymbol{\tau}$ pointing to the reader. Let $\phi(t) \in (-\pi, \pi]$ be the angle subtended by $-\mathbf{n}$ and \mathbf{h} , and $\varphi(t) \in (-\pi, \pi]$ is subtended by $-\mathbf{n}$ and the positive direction of x -axis. Without loss of generality, let the counter-clockwise direction of an angle be positive. Then, we have that $\phi(t) = \theta(t) - \varphi(t)$.

Now, we use $r(t)$ and $\phi(t)$ to denote the coordinates of the polar frame centered at the source position \mathbf{p}_o . It follows from (10) that

$$\begin{aligned} \dot{s}(t) &= -\alpha\dot{r}(t) = -\alpha v \cos \phi(t), \\ \dot{\phi}(t) &= \omega(t) - \frac{v}{r(t)} \sin \phi(t). \end{aligned} \quad (11)$$

One can easily observe from Fig. 2 that $\omega(t)$ should be designed such that $[s_d, -\pi/2]'$ is a stable equilibrium of (11) to achieve the objective (3). At equilibrium it follows that

$$\omega(t) = \omega_c = -v/r_d. \quad (12)$$

In the circumnavigation problem, ω_c is known for the controller design in Dong, You & Xie (2020). For the isoline tracking, this is not the case and we design an integrator $c_2\sigma(t)$ in (5) to estimate ω_c which is indispensable for the exact isoline tracking.

4.1 The P-like controller

Inserting (8) to (11) leads to that

$$\begin{aligned} \dot{s}(t) &= -\alpha v \cos \phi(t), \\ \dot{\phi}(t) &= c_1 \left(\dot{s}(t) + c_3 \tanh \left(\frac{\varepsilon(t)}{c_4} \right) \right) - \frac{v \sin \phi(t)}{r(t)}. \end{aligned} \quad (13)$$

One can show that (13) has two equilibria, one of which is unstable for any $c_{1,3,4} > 0$ and of no interest. The other one is $\tilde{\mathbf{x}}_e = [s_e, -\pi/2]'$ where $s_e = s_d - \alpha(r_e - r_d)$ and r_e is the unique solution of $g(r) = 0$ where

$$g(r) := -\tanh(\alpha(r - r_d)/c_4) + v/(c_1 c_3 r). \quad (14)$$

Then, we have the following result.

Lemma 2 Consider the equilibrium $\tilde{\mathbf{x}}_e$, it holds that

- (a) $s_e < s_d$ for any finite $c_1 > 0$.
- (b) $s_d - s_e$ decreases to zero as c_1 increases to infinity.

PROOF. By (14), the proof is trivial. ■

Although the P-like controller in (8) is unable to *exactly* complete the isoline tracking task, the tracking error can be arbitrarily reduced by increasing the controller gain c_1 , which is sufficient for application. We show below that the closed-loop system of (13) converges *globally* to $\tilde{\mathbf{x}}_e$.

Proposition 3 Consider the closed-loop system in (13) and let $\mathbf{x}(t) = [s(t), \phi(t)]'$. If the controller parameters are selected to satisfy that

$$c_1 > 0, \alpha v > c_3 > 0, c_4 > 0, \quad (15)$$

there exists a finite $t_1 > t_0$ such that

$$\|\mathbf{x}(t) - \tilde{\mathbf{x}}_e\| \leq C \|\mathbf{x}(t_1) - \tilde{\mathbf{x}}_e\| \exp(-\rho(t - t_1)), \forall t > t_1,$$

where ρ and C are two positive constants.

PROOF. See Appendix. ■

Remark 4 If $c_3 \geq v\alpha$, the Dubins vehicle either approaches the desired isoline $\mathcal{L}(s_d)$ with oscillations or diverges from it. Since α is an unknown parameter, the vehicle can collect N samples of $\dot{s}(t)$ and select c_3 such that

$$c_3 < \frac{1}{N} \cdot \sum_{i=1}^N |\dot{s}(i)| \leq \alpha v, \quad (16)$$

where i denotes the i -th sample.

By Lemma 2, the steady-state error $s_d - s_e$ cannot be eliminated for a finite c_1 . This is where the integrator $\sigma(t)$ comes into play in the next subsection.

4.2 The PI-like controller for the exact isoline tracking

Inserting (5) to (11), we obtain that

$$\begin{aligned} \dot{r}(t) &= v \cos \phi(t), \\ \dot{\phi}(t) &= -c_1 (\alpha \dot{r}(t) + c_3 \tanh(\alpha/c_4 \cdot (r(t) - r_d))) \\ &\quad + c_2 \sigma(t) - v \sin \phi(t)/r(t), \\ \dot{\sigma}(t) &= -\alpha \dot{r}(t) - c_3 \tanh(\alpha/c_4 \cdot (r(t) - r_d)). \end{aligned} \quad (17)$$

In (5), the integrator $\sigma(t)$, which is sometimes called the internal model (Khalil 2002, Chapter 12.3), is designed to enforce the tracking error to converge to zero. Together with (7), the objective in (3) is finally achieved. Unfortunately, we only obtain the local regulation via linearization. As the P-like controller is already able to arbitrarily reduce this error, we do not pursue the non-local regulation result for the PI-like controller.

Proposition 5 *Consider the isoline tracking system in (11) under the PI-like controller in (5). If the control parameters are selected to satisfy that*

$$c_1(c_1 - 2)v\alpha > c_2 \text{ and } v\alpha > c_3 > 0, \quad (18)$$

then $[r_d, -\pi/2, \omega_c/c_2]'$ is a locally exponentially stable equilibrium of (17).

PROOF. Clearly, $\mathbf{z}_e = [r_d, -\pi/2, \omega_c/c_2]'$ is an equilibrium of (17). Define an error vector

$$\begin{aligned} \mathbf{z}(t) &= [z_1(t), z_2(t), z_3(t)]' \\ &= [r(t) - r_d, \phi(t) + \pi/2, \sigma(t) - \omega_c/c_2]', \end{aligned}$$

and linearize (17) around \mathbf{z}_e . It follows that

$$\dot{\mathbf{z}}(t) = A\mathbf{z}(t), \quad (19)$$

where the Jacobian matrix A is given by

$$A = \begin{bmatrix} 0 & v & 0 \\ -c_1c_3\alpha/c_4 - \omega_c/r_d & -c_1v\alpha & c_2 \\ -c_3\alpha/c_4 & -v\alpha & 0 \end{bmatrix}.$$

Let $\mu_1 = c_1c_3\alpha/c_4 + \omega_c/r_d$, $\mu_2 = c_1\alpha(c_1\alpha v\mu_1 - c_2c_3\alpha/(2c_4))$, $\mu_3 = \mu_1v/2 + c_2\alpha v/2$, and $\mu_4 = c_1c_2c_4v\mu_1/c_3 - c_2^2/2$. Consider the following Lyapunov function candidate

$$V(\mathbf{z}) = \mathbf{z}'P\mathbf{z}, \quad (20)$$

where P is symmetric and obtained by

$$P = \frac{1}{2} \begin{bmatrix} 2\mu_2 + \mu_1^2 & c_1\alpha v\mu_1 & -c_2\mu_1 \\ c_1\alpha v\mu_1 & 2\mu_3 + (c_1\alpha v)^2 & -c_1c_2\alpha v \\ -c_2\mu_1 & -c_1c_2\alpha v & 2\mu_4 + c_2^2 \end{bmatrix}.$$

One can verify that the conditions in (18) ensure the positiveness of $V(\mathbf{z})$. Moreover,

$$V(\mathbf{z}) \leq \lambda_M(P)\|\mathbf{z}\|_2^2, \quad (21)$$

where λ_M denotes the maximum eigenvalue of P .

Then, taking the derivative of $V(\mathbf{z})$ in (20) along with (19) leads to that

$$\dot{V}(\mathbf{z}) = -\mathbf{z}'Q\mathbf{z} \text{ and } Q = \begin{bmatrix} q_{11} & 0 & 0 \\ 0 & q_{22} & q_{23} \\ 0 & q_{32} & q_{33} \end{bmatrix}, \quad (22)$$

where $q_{11} = c_1\alpha v\mu_1^2 - c_2c_3\alpha\mu_1/c_4$, $q_{22} = (c_1\alpha v)^3$, $q_{23} = c_2(c_1\alpha v)^2 - c_2^2\alpha v/2 + c_1c_2c_4(\alpha v)^2\mu_1/(c_3\alpha)$, $q_{32} = q_{23}$, and $q_{33} = c_1c_2^2\alpha v$. Clearly, Q is positive definite. It follows from (21) and (22) that

$$\dot{V}(\mathbf{z}) \leq -\lambda_m\|\mathbf{z}\|_2^2 \leq -\lambda_M^{-1}\lambda_m V(\mathbf{z}), \quad (24)$$

where λ_m denotes the minimum eigenvalue of Q . By the comparison principle (Khalil 2002, Lemma 3.4), \mathbf{z}_e is a locally exponentially stable equilibrium of (17). ■

5 The Isoline Tracking in Smoothing Fields

In this section, we extend the circular field to more general cases satisfying the following assumption.

Assumption 6 *The distribution function $F(\mathbf{p})$ is twice continuously differentiable, and for any compact set $\Omega \subseteq \mathbb{R}^2$ that excludes the stationary point of $F(\mathbf{p})$, there exist $\gamma_{1,2,3} > 0$ such that*

$$\gamma_1 \leq \|\nabla F(\mathbf{p})\| \leq \gamma_2, \quad \|\nabla^2 F(\mathbf{p})\| \leq \gamma_3, \quad \forall \mathbf{p} \in \Omega. \quad (25)$$

Remark 7 *Take the field in (9) as an example. Then,*

$$\|\nabla F(\mathbf{p})\| = \alpha F(\mathbf{p}) \text{ and } \|\nabla^2 F(\mathbf{p})\| = \alpha^2 F(\mathbf{p}),$$

when $\mathbf{p} \neq \mathbf{p}_0$. Obviously, (25) is satisfied.

Since s_d is not an extreme point of $F(\mathbf{p})$, it follows from Assumption 6 that the isoline $\mathcal{L}(s_d)$ is composed by multiple strictly separate closed curve, i.e.,

$$\mathcal{L}(s_d) = \bigcup_{i \in \mathcal{I}} \mathcal{C}_i$$

where \mathcal{I} is a countable set, the set \mathcal{C}_i is a closed curve and $\mathcal{C}_i \cap \mathcal{C}_j = \emptyset$ if $i \neq j$. If $F(\cdot)$ is further convex, $\mathcal{L}(s_d)$ contains only one closed curve. Otherwise, it may contain multiple disjoint closed curves, and the vehicle is expected to move along one of them, depending on the initial conditions.

In view of Fig. 2, we obtain that

$$\dot{s}(t) = -v\|\nabla F(\mathbf{p})\| \cos \phi(t). \quad (26)$$

Taking the derivative of $\dot{s}(t)$ leads to that

$$\begin{aligned}\ddot{s}(t) &= \omega(t)v\mathbf{n}'\boldsymbol{\tau} + v^2\mathbf{h}'\nabla^2 F(\mathbf{p})\mathbf{h} \\ &= \omega(t)v\|\nabla F(\mathbf{p})\| \sin \phi(t) + v^2\mathbf{h}'\nabla^2 F(\mathbf{p})\mathbf{h}.\end{aligned}\quad (27)$$

By Fig. 2, $\mathbf{x}_e = [s_d, -\pi/2]'$ is also the desired equilibrium of (26). Suppose that $\mathbf{x}(t) = \mathbf{x}_e$, it follows from (27) that

$$\ddot{s}(t) = -\omega(t)v\|\nabla F(\mathbf{p})\| + v^2\mathbf{h}'\nabla^2 F(\mathbf{p})\mathbf{h}.$$

To maintain $\ddot{s}(t) = 0$, it requires that

$$\omega(t) = \frac{v\mathbf{h}'\nabla^2 F(\mathbf{p})\mathbf{h}}{\|\nabla F(\mathbf{p})\|}, \quad (28)$$

which is time-varying and different from the case of the circular field of (9). Since $F(\cdot)$ is unknown, we cannot use (28), which renders it impossible to exactly complete the isoline tracking task. Instead, we are able to design the P-like controller in (8) such that $|\varepsilon(t)|$ is uniformly bounded, and the bound can be arbitrarily reduced by increasing the P gain c_1 .

Proposition 8 *Consider the isoline tracking system in (26) and (27) under the P-like controller in (8). Suppose that Assumption 6 holds and there is a closed curve in $\mathcal{L}(s_d)$ such that $\phi(t_0) \in [-\epsilon, -\pi + \epsilon]$ where $\epsilon \in (0, \pi/2)$. Let the control parameters be selected to satisfy that*

$$c_1 > \max \left\{ \frac{\gamma_3 v}{\gamma_1 \sin \epsilon (v\gamma_1 \cos \epsilon - c_3)}, \frac{c_4 \gamma_3 v + c_3 \gamma_2}{c_3 \gamma_1 \sin \epsilon} \right\},$$

and $0 < c_3 < v\gamma_1 \cos \epsilon$, then

$$\lim_{t \rightarrow \infty} |s(t) - s_d| \leq \tanh^{-1} \left(\frac{c_4 \gamma_3 v + c_3 \gamma_2}{c_1 c_3 \gamma_1 \sin \epsilon} \right).$$

The proof depends on the following technical result.

Lemma 9 *Consider the following system*

$$\dot{z}(t) = -k \tanh(z(t)) + b. \quad (29)$$

If $k > b > 0$, then $\limsup_{t \rightarrow \infty} |z(t)| \leq \tanh^{-1}(b/k)$.

PROOF. Consider a Lyapunov function candidate as

$$V_z(z) = 1/2 \cdot z^2(t).$$

Taking the derivative of $V_z(z)$ along with (29) leads to that

$$\begin{aligned}\dot{V}_z(z) &= z(t) (-k \tanh(z(t)) + b) \\ &\leq -kz(t) \tanh(z(t)) + b|z(t)|.\end{aligned}$$

Since $k > b > 0$, it holds that $\dot{V}_z(z) \leq 0$ for all $|z(t)| \geq \tanh^{-1}(b/k)$. This completes the proof. ■

PROOF. [Proof of Proposition 8] Firstly, we show that $\phi(t)$ cannot escape from the region $[-\epsilon, -\pi + \epsilon]$. To this end, inserting the P-like controller (8) to (27) leads to that

$$\ddot{s}(t) = c_1 v \mathbf{n}' \boldsymbol{\tau} (\dot{s}(t) + c_3 \tanh(\varepsilon(t)/c_4)) + v^2 \mathbf{h}' \nabla^2 F(\mathbf{p}) \mathbf{h}. \quad (30)$$

When $\phi(t) = -\epsilon$, it follows from (30) that

$$\begin{aligned}\ddot{s}(t) &= v^2 \mathbf{h}' \nabla^2 F(\mathbf{p}) \mathbf{h} - c_1 v \|\nabla F(\mathbf{p})\| \sin \epsilon \times \\ &\quad (v \|\nabla F(\mathbf{p})\| \cos \epsilon + c_3 \tanh(\varepsilon(t)/c_4)) \\ &\leq -c_1 v \gamma_1 \sin \epsilon (v \gamma_1 \cos \epsilon - c_3) + \gamma_3 v^2 \\ &< 0.\end{aligned}\quad (31)$$

Similarly, $\phi(t) = -\pi + \epsilon$ leads to that

$$\ddot{s}(t) \geq -c_1 v \gamma_1 \sin \epsilon (-v \gamma_1 \cos \epsilon + c_3) - \gamma_3 v^2 > 0. \quad (32)$$

Since $\dot{s}(t)$ and $\phi(t)$ are continuous in t , then $\phi(t)$ will stay in the region $[-\epsilon, -\pi + \epsilon]$ if $\phi(t_0) \in [-\epsilon, -\pi + \epsilon]$.

Consider a Lyapunov function candidate as

$$V_e(e) = 1/2 \cdot e^2(t).$$

Taking the derivative of $V_e(e)$ along with (26) and (30) leads to that

$$\begin{aligned}\dot{V}_e(e) &= e(t) (\ddot{s}(t) + c_3/c_4 \cdot (1 - \tanh^2(\varepsilon(t)/c_4)) \dot{s}(t)) \\ &= c_1 v \mathbf{n}' \boldsymbol{\tau} e^2(t) + e(t) \times \\ &\quad (v^2 \mathbf{h}' \nabla^2 F(\mathbf{p}) \mathbf{h} + c_3/c_4 \cdot (1 - \tanh^2(\varepsilon(t)/c_4)) \dot{s}(t)) \\ &\leq c_1 v \mathbf{n}' \boldsymbol{\tau} e^2(t) + (\gamma_3 v^2 + c_3/c_4 \cdot \gamma_2 v) |e(t)| \\ &\leq -(c_1 v \gamma_1 \sin \epsilon) e^2(t) + (\gamma_3 v^2 + c_3/c_4 \cdot \gamma_2 v) |e(t)|.\end{aligned}$$

It is clear that $\dot{V}_e(e) \leq 0$ holds for all

$$|e(t)| \geq \eta := \frac{\gamma_3 v + c_3 \gamma_2 / c_4}{c_1 \gamma_1 \sin \epsilon}.$$

Thus, $|e(t)|$ will be eventually bounded by η , i.e.,

$$\lim_{t \rightarrow \infty} |\dot{s}(t) + c_3 \tanh(\varepsilon(t)/c_4)| \leq \eta.$$

By Lemma 9 and the condition that $c_1 > \frac{c_4 \gamma_3 v + c_3 \gamma_2}{c_3 \gamma_1 \sin \epsilon}$, it implies

$$\lim_{t \rightarrow \infty} |s(t) - s_d| \leq \tanh^{-1} \left(\frac{c_4 \gamma_3 v + c_3 \gamma_2}{c_1 c_3 \gamma_1 \sin \epsilon} \right).$$

This completes the proof. ■

6 Extension to Other Vehicles

In this section, we further extend the PI-like controller (5) for the Dubins vehicle (4) to the cases of a single-integrator vehicle and a double-integrator vehicle, respectively.

6.1 Controller design for single-integrator vehicles

Consider a single-integrator vehicle as follows

$$\dot{\mathbf{p}}_1(t) = \mathbf{v}_1(t), \quad (33)$$

where $\mathbf{p}_1(t)$ and $\mathbf{v}_1(t)$ denote the position and velocity of the single-integrator vehicle in 2-D, respectively.

To complete the isoline tracking task in (3) by the single-integrator vehicle (33), we propose a *concentration-only* controller

$$\mathbf{v}_1(t) = v \begin{bmatrix} \cos \theta_1(t) \\ \sin \theta_1(t) \end{bmatrix}', \quad (34)$$

where v is the constant linear speed and $\theta_1(t)$ is given as

$$\theta_1(t) = c_1 s(t) + c_1 c_3 \zeta(t), \quad \dot{\zeta}(t) = \tanh(\varepsilon(t)/c_4). \quad (35)$$

Taking the time derivative of $\theta_1(t)$ leads to that

$$\dot{\theta}_1(t) = c_1 \dot{s}(t) + c_1 c_3 \tanh(\varepsilon(t)/c_4) = c_1 e(t),$$

which is of the same as the P-like controller (5). In this case, the trajectories of the Dubins vehicle (4) and single-integrator vehicle (33) are identical if they have same initial states, as shown in Lemma 10.

Lemma 10 *Consider the Dubins vehicle (4) under the P-like controller in (8) and the single-integrator vehicle (33) under the controller (35). If the two vehicles start at the same initial states, i.e., $\mathbf{p}(t_0) = \mathbf{p}_1(t_0)$ and $\theta(t_0) = \theta_1(t_0)$, then their trajectories are identical.*

PROOF. Define an error vector as follows

$$\mathbf{z}(t) = [\mathbf{p}'(t) - \mathbf{p}'_1(t), \theta(t) - \theta_1(t)]'. \quad (36)$$

If the Dubins vehicle (4) and the single-integrator vehicle (33) have the same state at some time t , e.g., $\mathbf{z}(t) = \mathbf{0}$, it further holds that

$$\dot{\mathbf{z}}(t) = [\mathbf{v}'(t) - \mathbf{v}'_1(t), \dot{\theta}(t) - \dot{\theta}_1(t)]' = \mathbf{0},$$

where $\mathbf{v}(t) = v[\cos \theta(t), \sin \theta(t)]'$ is the velocity of the Dubins vehicle. Thus, the trajectories of the vehicles (4) and (37) are identical if they have same initial states. ■

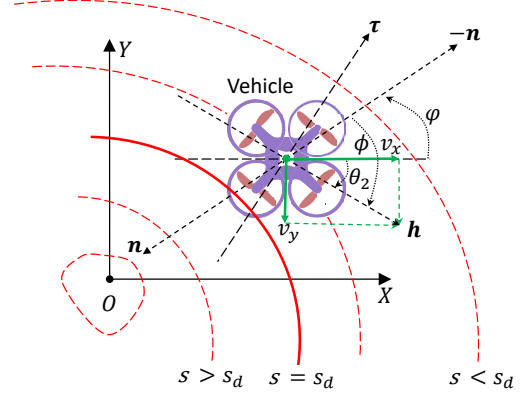


Fig. 3. Coordinates of the double-integrator vehicle in scalar fields.

6.2 Controller design for double-integrator vehicles

Consider a double-integrator vehicle in Fig. 3

$$\dot{\mathbf{p}}_2(t) = \dot{\mathbf{v}}_2(t) \text{ and } \dot{\mathbf{v}}_2(t) = \mathbf{a}_2(t), \quad (37)$$

where $\mathbf{p}_2(t)$, $\mathbf{v}_2(t) = [v_x(t), v_y(t)]'$, and $\mathbf{a}_2(t)$ denote the position, velocity, and acceleration in 2-D, respectively.

We propose the following controller

$$\mathbf{a}_2(t) = \underbrace{\omega(t) \begin{bmatrix} -v_y(t) \\ v_x(t) \end{bmatrix}}_{\text{For isoline tracking}} + \underbrace{c_5 \cdot \text{sgn}(\mathbf{v}_2^d(t) - \mathbf{v}_2(t))}_{\text{For velocity regulation}}, \quad (38)$$

where $\text{sgn}(\mathbf{x})$ returns the sign of each element of \mathbf{x} , $c_5 > 0$ is the control parameter to be determined, $\omega(t)$ is the PI-like controller in (5), the desired velocity is decomposed as

$$\mathbf{v}_2^d(t) = v[\cos \theta_2(t), \sin \theta_2(t)]',$$

and $\theta_2(t) = \arctan(v_y(t)/v_x(t))$ in Fig. 3.

In (38), the first term is orthogonal to $\mathbf{v}_2(t)$ and is used to complete the isoline task and the other aims to regulate the velocity $\mathbf{v}_2(t)$ such that

$$v_2(t) = v, \quad \forall t > t_0 + T,$$

where $v_2(t) = \|\mathbf{v}_2(t)\|_2$ is the linear speed of the double-integrator vehicle, and $T > 0$ is finite.

Lemma 11 *Consider the double-integrator in (37) under the controller (38), there is a finite $T > 0$ such that*

$$v_2(t) = v, \quad \forall t > t_0 + T.$$

PROOF. Consider the following Lyapunov function

$$V_v(v_2) = 1/2 \cdot (v_2(t) - v)^2.$$

Taking the derivative of $V_v(v_2)$ along with (37) and (38) leads to that

$$\begin{aligned} \dot{V}_v(v_2) &= 1/v_2(t) \cdot (v_2(t) - v) (v_x(t)\dot{v}_x(t) + v_y(t)\dot{v}_y(t)) \\ &= -c_5|v_2(t) - v| (|\cos \theta_2(t)| + |\sin \theta_2(t)|) \\ &\leq -c_5|v_2(t) - v| \\ &= -\sqrt{2}c_5V_v^{1/2}(v_2). \end{aligned}$$

By the comparison principle, it follows that

$$v_2(t) = v, \forall t > t_0 + T,$$

where $T = \sqrt{2}V_v^{1/2}(v_2(t_0))/c_5$. ■

After a finite time of length T , the double-integrator vehicle in (37) is only controlled by the first term of (38)

$$\mathbf{a}_2(t) = \omega(t)[-v_y(t), v_x(t)]'. \quad (39)$$

Since the above is orthogonal to $\mathbf{v}_2(t)$, we can show that the trajectories of the two vehicles (5) and (37) are identical if they have same initial states.

Lemma 12 Consider the Dubins vehicle (4) under the PI-like controller (5) and the double-integrator vehicle (37) under the controller (38). If the two vehicles have same initial states, i.e., $\mathbf{p}(t_0) = \mathbf{p}_2(t_0)$, $v_2(t_0) = v$, and $\theta(t_0) = \theta_2(t_0)$, their trajectories are identical.

PROOF. Similar to (36), we define an error vector as

$$\mathbf{z}(t) = [\mathbf{p}'(t) - \mathbf{p}'_2(t), \mathbf{v}'(t) - \mathbf{v}'_2(t)]',$$

where $\mathbf{v}(t) = v[\cos \theta(t), \sin \theta(t)]'$. If the Dubins vehicle (4) and double-integrator vehicle (37) have same states at some time t , it holds that $\mathbf{z}(t) = \mathbf{0}$ and $\dot{\mathbf{z}}(t) = \mathbf{0}$. Thus, the trajectories of the vehicles (4) and (37) are identical if they have same initial states. ■

7 Simulations

In this section, the effectiveness and advantages of the proposed controllers are validated by simulations. Particularly, the PI-like controller (5) and the controller (37) are performed on the simulators of (a) a 6-DOF fixed-wing UAV in the field of PM2.5; and (b) a quadrotor built by CrazyFlie 2.0 platform, respectively.

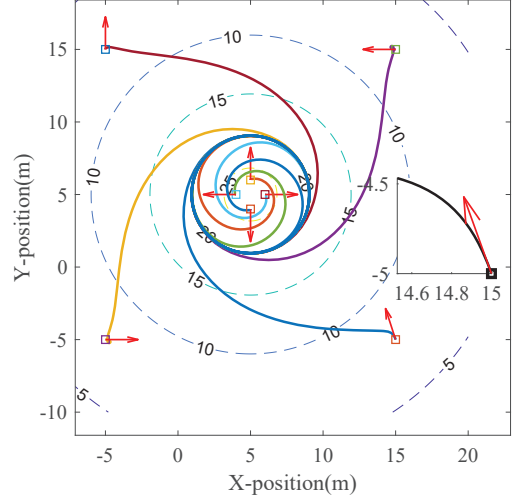


Fig. 4. Trajectories of the Dubins vehicle with different initial states.

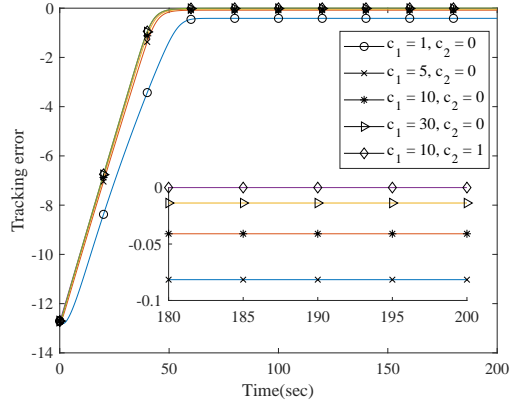


Fig. 5. Tracking errors with different control parameters.

7.1 The isoline tracking in a circular field

Consider the Dubins vehicle in (4), and let $\beta(t) = [\mathbf{p}'(t), \theta(t)]'$ denote its state. The linear speed is set as $v = 0.5$ m/s and the circular field of (9) is

$$F(\mathbf{p}) = 30 \exp\left(-0.1\sqrt{(x-5)^2 + (y-5)^2}\right). \quad (40)$$

The control parameters of the PI-like controller (5) is given in Table 1. Fig. 4 illustrates the field distribution of (40) and the trajectories under different initial states: $\beta(t_0) = [15, -5, 0.6\pi]'$, $[15, 15, \pi]'$, $[-5, 15, \pi/2]'$, $[-5, -5, 0]'$, $[6, 5, 0]'$, $[5, 6, \pi/2]'$, $[4, 5, \pi]'$, and $[5, 4, -\pi/2]'$. Fig. 5 depicts the tracking errors and confirms that increasing c_1 can reduce the tracking error and only the PI-like controller with $c_2 = 1$ exactly achieves the objective in (3). Fig. 6 validates that the integrator $c_2\sigma(t)$ converges to $\omega_c = -v/r_d$.

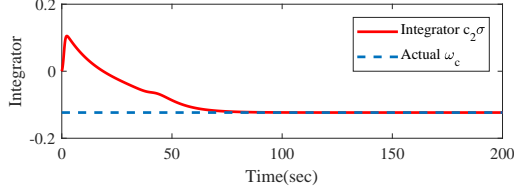


Fig. 6. The integrator $c_2\sigma(t)$ and $\omega_c = -v/r_d$.

Table 1
Parameters of the PI-like controller (5) in Section 7.1

Parameter	c_1	c_2	c_3	c_4
Value	10	1	0.3	1

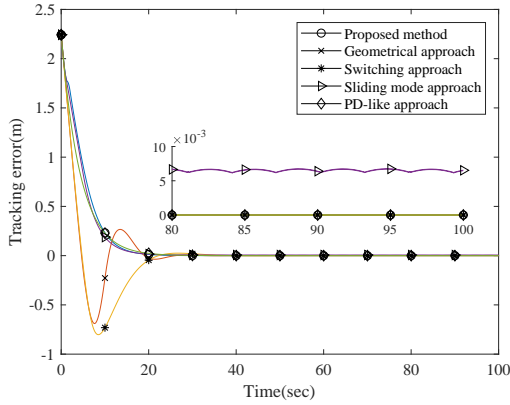


Fig. 7. Comparison with the existing methods.

Table 2
Parameters of the PI-like controller (5) in Section 7.3

Parameter	c_1	c_2	c_3	c_4
Value	10	0	0.1	1

7.2 Comparison with other controllers for circumnavigation

We compare our PI-like controller (5) with other methods in the context of circumnavigation including (a) the geometrical approach (Cao 2015) with parameters $k = 1$ and $r_a = 9.95$; (b) the switching approach (Zhang et al. 2017) with $k = 1.4/r_d$; (c) the sliding mode approach (Matveev et al. 2011) with $\delta = 0.83$ and $\gamma = 0.3$; and (d) the PD-like approach (Dong, You & Xie 2020) with $c_1 = 200$ and $c_2 = 30$. In Fig. 7, one can observe that both the geometrical approach and the switching approach have large overshoots. The sliding mode approach cannot exactly complete the isoline tracking problem and the performance of the PI-like controller is almost of the same as the PD-like approach, which however requires to know $\omega_c = -v/r_d$ and thus cannot be applied to the isoline tracking problem of this work.

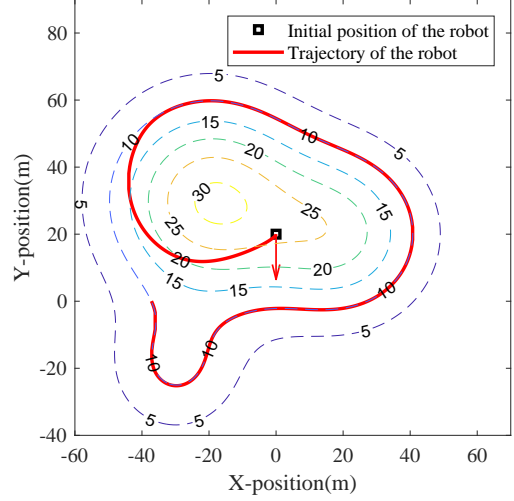


Fig. 8. Fields distribution and trajectory of the Dubins vehicle.

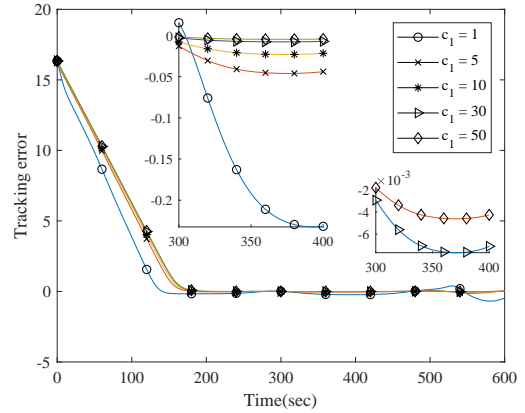


Fig. 9. Tracking errors of the Dubins vehicle with different proportional gain c_1 .

7.3 The isoline tracking in a smoothing field

Consider the following scalar field (Matveev et al. 2012)

$$F(\mathbf{p}) = 20 \exp\left(-\frac{((x-20)^2 + (y-20)^2)}{600}\right) + 30 \exp\left(-\frac{((x+30)^2 + (y+20)^2)}{400}\right) + 10 \exp\left(-\frac{((x+20)^2 + (y-30)^2)}{800}\right). \quad (41)$$

The field distribution and the trajectory of the Dubins vehicle under the PI-like controller (5) with parameters in Table 2 are illustrated in Fig. 8, where $\beta(t_0) = [0, 20, -\pi/2]$ and $s_d = 10$. Fig. 9 depicts the tracking errors with $c_1 = 1, 5, 10, 30, 50$. Clearly, we can reduce the steady-state error by increasing c_1 which is consistent with Proposition 8. Fig. 10 validates that the single-integrator vehicle (33) under the controller (35) produce similar trajectory as the Dubins vehicle.

Then, a 6-DOF quadrotor under the controller in (38) is included to complete the objective (3) in the field of

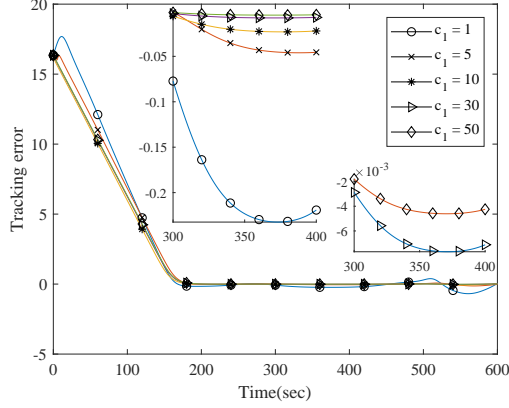


Fig. 10. Tracking errors of the single-integrator vehicle with different proportional gain c_1 .

Table 3
Parameters of the PI-SM controller (38)

Parameter	c_1	c_2	c_3	c_4	c_5
Value	30	0.1	0.1	1	0.1

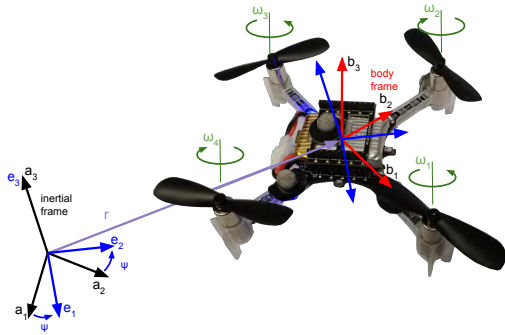


Fig. 11. CrazyFlie 2.0 quadrotor (Lu 2017).

(41). The simulator of the quadrotor is directly obtained from Lu (2017), which is built via CrazyFlie 2.0 platform made by Bitcraze, see Fig. 11 and Lu (2017) for details. The control parameters for (38) are given in Table 3, and the tracking error and speed of the quadrotor are illustrated in Fig. 12. Moreover, the desired isoline and speed are set as $s_d = 10$ and $v = 0.5$. By the partially enlarged view of Fig. 12, one can observe that $v_2(t)$ converges to v in a short time. Note that the altitude and attitude of the quadrotor are controlled by the original controller of Lu (2017).

7.4 The isoline tracking in a field of PM2.5 by a fixed-wing UAV

In this subsection, a 6-DOF fixed-wing UAV (Beard & McLain 2012) is adopted to test the effectiveness of the PI-like controller (5) in the field of PM2.5, see Figs. 1 and 13. Due to page limitation, we omit details of the mathematical model of the UAV, which can be found in Beard & McLain (2012), and adopt codes from Lee

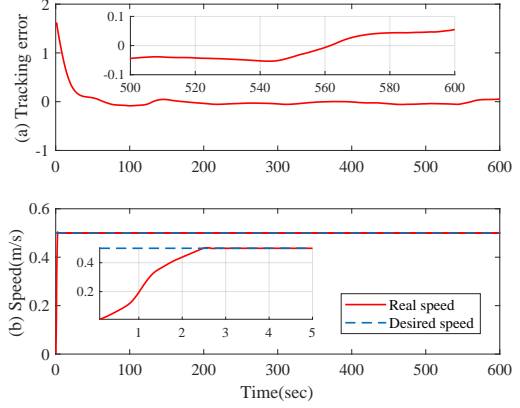


Fig. 12. Tracking error and linear speed of the quadrotor.

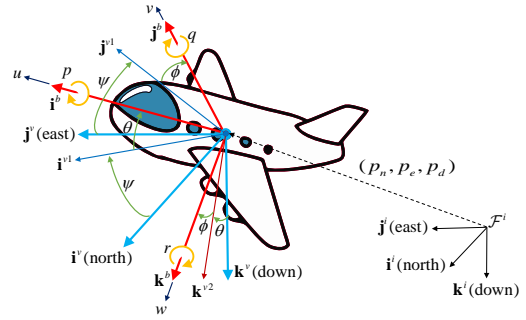


Fig. 13. Coordinates of the fixed-wing 6-DOF UAV (Dong, You & Xie 2020).

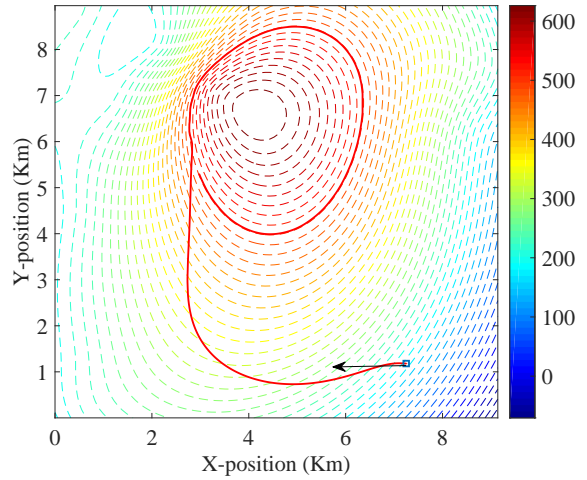


Fig. 14. Trajectory of the fixed-wing UAV in the field of PM 2.5.

(2016) for the model. The sampling frequency for the PM2.5 is set as 1 Hz and the linear speed of the UAV is maintained as 30 m/s (Lee 2016). Fig. 14 depicts the distribution of the field and the trajectory of the UAV, where the square and arrow denote its initial position and course. Fig. 15 illustrates the tracking error $\varepsilon(t)$ and the derivative of concentration $\dot{s}(t)$ versus time, which completes the isoline tracking task.

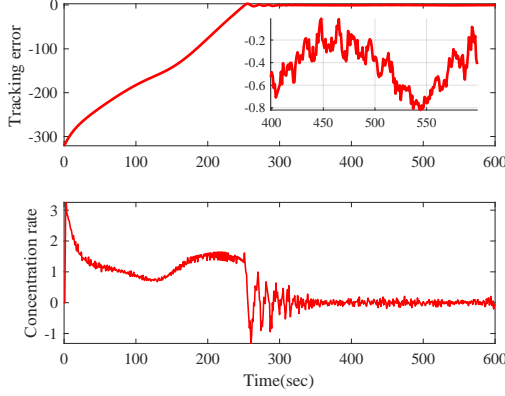


Fig. 15. Tracking error $\varepsilon(t)$ and derivative of concentration $\dot{s}(t)$ of the fixed-wing UAV.

8 Conclusion

To track a desired isoline of a smoothing scalar field, we have designed a coordinate-free controller in a PI-like form for a Dubins vehicle by using concentration-based measurements in this work. A novel idea lies in the design of a sliding surface based error in the standard PI controller. Moreover, we have extended the PI-like controller to the cases of a single-integrator vehicle and a double-integrator vehicle, respectively. Finally, the simulation results have validated our theoretical finding.

Appendix. Proof of Proposition 3

To prove Proposition 3, we first show that the closed-loop system in (13) asymptotically converges if $\phi(t_0) \in [-\pi, 0]$ in Lemma 13. Then, we show its local exponential stability in Lemma 14. Finally, we prove that there exists a finite time instant $t_1 \geq t_0$ such that $\phi(t) \in [-\pi, 0]$, $\forall t \geq t_1$ for any initial state in Lemma 15.

Lemma 13 *Under the conditions in Proposition 3, if $\phi(t_0) \in [-\pi, 0]$, then*

$$\lim_{t \rightarrow \infty} |s(t) - s_e| = \lim_{t \rightarrow \infty} |\dot{s}(t)| = 0. \quad (42)$$

PROOF. Similar to the proof of Proposition 8, we need to verify that $\phi(t)$ remains in the region $[-\pi, 0]$, if $\phi(t_0) \in [-\pi, 0]$. If $\phi(t) = 0$, it follows from (13) that

$$\dot{\phi}(t) = c_1(\alpha v + c_3 \tanh(\varepsilon(t)/c_4)) \geq c_1(\alpha v - c_3) > 0.$$

Similarly, $\phi(t) = -\pi$ leads to that

$$\dot{\phi}(t) \leq c_1(-\alpha v + c_3) < 0.$$

Since $\dot{\phi}(t)$ is continuous in t , we obtain that $\phi(t) \in [-\pi, 0]$, $\forall t > t_0$.

Let $\mathbf{y}(t) = [r(t), \phi(t)]'$ and $\mathbf{y}_e = [r_e, -\pi/2]'$, where r_e denotes the distance from the vehicle to the source position \mathbf{p}_0 if $s(t) = s_e$.

Consider a Lyapunov function candidate as

$$V(\mathbf{y}) = \frac{1}{v} \int_{r_e}^{y_1(t)} \left(c_1 c_3 \tanh\left(\frac{\alpha(\tau - r_d)}{c_4}\right) - \frac{v}{\tau} \right) d\tau + 1 + \sin y_2(t).$$

Taking the time derivative of $V(\mathbf{y})$ leads to that

$$\begin{aligned} \dot{V}(\mathbf{y}) &= \left(c_1 c_3 \tanh\left(\frac{\alpha(y_1(t) - r_d)}{c_4}\right) - \frac{v}{y_1(t)} \right) \cos y_2(t) \\ &\quad + (\omega(t) - v \sin y_2(t)/y_1(t)) \cos y_2(t) \quad (43) \\ &= -v \cos y_2(t) \left(c_1 \alpha \cos y_2(t) + \frac{\sin y_2(t)}{y_1(t)} + \frac{1}{y_1(t)} \right). \end{aligned}$$

(a) If $y_2(t) \in [-\pi/2, 0]$, then $\cos y_2(t) \geq 0$ and

$$\sin y_2(t)/y_1(t) + 1/y_1(t) \geq 0,$$

which implies that $\dot{V}(\mathbf{y}) \leq 0$.

(b) If $y_2(t) \in [-\pi, -\pi/2]$, then $\cos y_2(t) < 0$, and three cases are considered separately to check the sign of $\dot{V}(\mathbf{y})$.

(i) If $y_1(t) \geq r_d$, then

$$c_1 \alpha \cos y_2(t) < \cos y_2(t)/r_d \leq \cos y_2(t)/y_1(t).$$

Together with $\cos y_2(t) + \sin y_2(t) + 1 < 0$, it holds that $\dot{V}(\mathbf{y}) < 0$.

(ii) If $1/(c_1 \alpha) < y_1(t) < r_d$, then

$$y_1(t) > \frac{1}{c_1 \alpha} > \frac{1}{c_1 \alpha} \left(\frac{1 + \sin y_2(t)}{-\cos y_2(t)} \right)$$

and $\dot{V}(\mathbf{y}) < 0$.

(iii) If $0 < y_1(t) \leq 1/(c_1 \alpha)$, it follows from (13) that

$$\dot{y}_2(t) > -c_1 \alpha v \cos y_2(t) - c_1 \alpha v \sin y_2(t) > c_1 \alpha v > 0.$$

Thus, $y_2(t)$ will monotonically increase until entering $[-\pi/2, 0]$, which is Case (a). Moreover, when $y_2(t) = -\pi/2$, it holds that

$$\begin{cases} \dot{y}_2(t) < 0, & \text{if } y_1(t) > r_e, \\ \dot{y}_2(t) = 0, & \text{if } y_1(t) = r_e, \\ \dot{y}_2(t) > 0, & \text{if } y_1(t) < r_e. \end{cases}$$

That is, the vehicle never return to Case (iii). Finally, we have $\dot{V}(\mathbf{y}) < 0$.

Let $\mathcal{S} = \{\mathbf{y} | \dot{V}(\mathbf{y}) = 0\}$. For any $\tilde{\mathbf{y}}_e \in \mathcal{S}$ and $\tilde{\mathbf{y}}_e \neq \mathbf{y}_e$, then $\dot{y}_2|_{\mathbf{y}=\tilde{\mathbf{y}}_e} = c_1 c_3 \tanh(\varepsilon(t)/c_4) + v/y_1(t) \neq 0$. Thus, no solution can stay identically in \mathcal{S} other than $\mathbf{y}(t) \equiv \mathbf{y}_e$. Note that $V(\mathbf{y})$ is nonnegative, and $V(\mathbf{y}) > 0, \forall \mathbf{y} \neq \mathbf{y}_e$. By the LaSalle's invariance theorem (Khalil 2002, Corollary 4.1), \mathbf{y}_e is an asymptotically stable equilibrium of the closed-loop system in (11) under the P-like controller (8), i.e., $\lim_{t \rightarrow \infty} \mathbf{x}(t) = \tilde{\mathbf{x}}_e$, which is implied by (10). ■

Lemma 14 *Under the conditions in Proposition 3, if $\phi(t_0) \in [-\pi, 0]$, then there is a finite $t_1 \geq t_0$ such that*

$$\|\mathbf{x}(t) - \tilde{\mathbf{x}}_e\| \leq C \|\mathbf{x}(t_1) - \tilde{\mathbf{x}}_e\| \exp(-\rho(t - t_1)), \forall t > t_1,$$

where ρ and C are two positive constants.

PROOF. Firstly, we define $\mathbf{x}(t) = [x_1(t), x_2(t)]'$ and recall the closed-loop system in (13) that

$$\begin{aligned} \dot{x}_1(t) &= -\alpha v \cos x_2(t), \\ \dot{x}_2(t) &= c_1 (\dot{x}_1(t) + c_3 \tanh((x_1(t) - s_d)/c_4)) \\ &\quad + \alpha v \sin x_2(t) / (\alpha r_d + s_d - x_1(t)). \end{aligned} \quad (44)$$

Linearizing (44) around $\tilde{\mathbf{x}}_e$ leads to that

$$\dot{\mathbf{x}}(t) = \tilde{A}(\mathbf{x}(t) - \tilde{\mathbf{x}}_e) \text{ and } \tilde{A} = \begin{bmatrix} 0 & -\alpha v \\ a_{21} & -c_1 \alpha v \end{bmatrix}, \quad (45)$$

where

$$a_{21} = \frac{c_1 c_3}{c_4} \left(1 - \tanh^2 \left(\frac{s_e - s_d}{c_4} \right) \right) - \frac{\alpha v}{(\alpha r_d + s_d - s_e)^2}.$$

Obviously, both the eigenvalues of \tilde{A} have negative real part, i.e., \tilde{A} is Hurwitz. Let

$$\mathcal{D} = \{\mathbf{x} | V(\mathbf{x}) \leq b\}, \quad (46)$$

where $b > 0$. If b is sufficiently small, then $x_1(t)$ is sufficiently close to s_e and $x_2(t)$ is sufficiently close to $-\pi/2$.

By Lemma 13, there exists a finite t_1 such that $\mathbf{x}(t) \in \mathcal{D}$ for all $t > t_1$. Then, it follows from (45) that the trajectory of the system satisfies

$$\mathbf{x}(t) - \tilde{\mathbf{x}}_e = G \exp(\Lambda(t - t_1)) G^{-1} (\mathbf{x}(t_1) - \tilde{\mathbf{x}}_e), \forall t > t_1,$$

where $\tilde{A} = G \Lambda G^{-1}$, $\Lambda = \text{diag}(\lambda_1, \lambda_2)$, and $\lambda_i, i = 1, 2$ are the eigenvalues of matrix \tilde{A} . Finally, it holds that

$$\begin{aligned} \|\mathbf{x}(t) - \tilde{\mathbf{x}}_e\| &= \|G \exp(\Lambda(t - t_1)) G^{-1} (\mathbf{x}(t_1) - \tilde{\mathbf{x}}_e)\| \\ &\leq C \|\mathbf{x}(t_1) - \tilde{\mathbf{x}}_e\| \exp(-\rho(t - t_1)), \end{aligned}$$

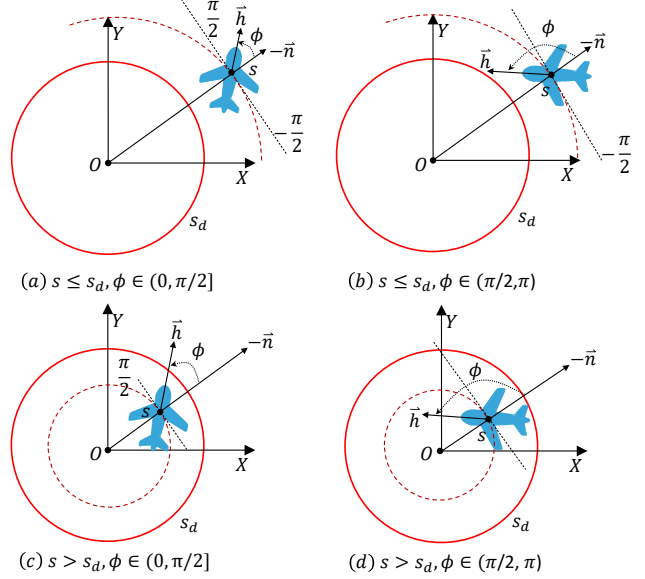


Fig. 16. Illustrations of the state of the Dubins vehicle.

where $C = \|G\| \|G^{-1}\|$, $\Delta = (c_1 \alpha v)^2 - 4a_{21} \alpha v$, and

$$\rho = \begin{cases} (c_1 \alpha v - \sqrt{\Delta})/2, & \text{if } \Delta > 0, \\ c_1 \alpha v/2, & \text{if } \Delta \leq 0. \end{cases}$$

■

Lemma 15 *Under the conditions in Proposition 3, there exists a finite $t_1 > t_0$ such that $\phi(t_1) \in [-\pi, 0]$ for any initial state $\phi(t_0) \in (0, \pi)$.*

PROOF. To prove Lemma 15, four cases in Fig. 16 are considered.

For the case in Fig. 16(a), i.e., $s(t_0) \in (0, s_d]$ and $\phi(t_0) \in (0, \pi/2]$, it follows from (13) that $\dot{s}(t_0) \leq 0$ and

$$\begin{aligned} \dot{\phi}(t_0) &= c_1 (\dot{s}(t_0) + c_3 \tanh(\varepsilon(t_0)/c_4)) - v \sin \phi(t_0)/r(t_0) \\ &< -c_1 \alpha v \cos \phi(t_0) < 0. \end{aligned}$$

Since $\phi(t)$ is continuous in t , $\phi(t)$ will monotonically decrease until $\phi(t_0 + \delta) \in [-\pi, 0]$ where $\delta > 0$ is finite.

For the case in Fig. 16(b), i.e., $s(t_0) \in (0, s_d]$ and $\phi(t_0) \in (\pi/2, \pi)$, it follows from (13) that

$$\begin{cases} \dot{\phi}(t) < 0, & \text{if } \phi(t) = \pi/2, \\ \dot{\phi}(t) > 0, & \text{if } \phi(t) = \pi. \end{cases}$$

Then, there are three possible results after some finite time $\delta > 0$: (i) $\phi(t_0 + \delta) \geq \pi$ and $s(t_0 + \delta) \leq s_d$, which is equivalent to that $\phi(t_0 + \delta) \geq -\pi$; (ii) $\phi(t_0 + \delta) \leq \pi/2$ and $s(t_0 + \delta) \leq s_d$, which is the case in Fig. 16(a);

(iii) $s(t_0 + \delta) > s_d$, which corresponds to the cases in Fig. 16(c) and (d).

Next, we show that $\phi(t)$ will enter the region $[-\pi, 0]$ in finite time. When $\phi(t) = \pi/2$ and $s(t) > s_d$, it follows from (13) that

$$\dot{\phi}(t) = c_1 c_3 \tanh(-\alpha/c_4 \cdot (r(t) - r_d)) - v/r(t).$$

- (a) If there is no solution in the region $(0, r_d)$ such that $\dot{\phi}(t) = 0$, then $\phi(t)$ is monotonic in the cases of Fig. 16(c) and (d).
- (b) If there is a solution $0 < r_* < r_d$ such that $\dot{\phi}(t) = 0$, the equilibrium $\mathbf{y}_* = [r_*, \pi/2]'$ is unstable and there is no closed orbit around it.

Overall, there are two possible results after some finite $\delta > 0$: (i) $r(t_0 + \delta) \geq r_d$ and $\phi(t_0 + \delta) \in (0, \pi/2]$, which is Fig. 16(a); (ii) $\phi(t_0 + \delta) \in [-\pi, 0]$. Thus, we conclude that there exists a finite time instant $t_1 > t_0$ such that $\phi(t_1) \in [-\pi, 0]$ for any initial $\phi(t_0) \in (0, \pi)$.

To elaborate (b), we linearize (13) around \mathbf{y}_* as

$$\dot{\mathbf{y}}(t) = A_*(\mathbf{y}(t) - \mathbf{y}_*) \text{ and } A_* = \begin{bmatrix} 0 & -v \\ a_{21}^* & c_1 \alpha v \end{bmatrix},$$

where $a_{21}^* = -\frac{c_1 c_3 \alpha}{c_4} \left(1 - \tanh^2\left(\frac{\alpha(r_* - r_d)}{c_4}\right)\right) + \frac{v}{r_*^2}$. It is clear that A_* at least has one unstable eigenvalue. Then, we show that there is no closed orbit around \mathbf{y}_* by applying Dulac's Criterion (Strogatz 2018, Section 7.2) and selecting a continuously differentiable, real-value function $h(\mathbf{y}) = y_1(t)$. If $y_1(t) \in (0, r_d)$ and $y_2(t) \in (0, \pi)$, it holds that

$$\frac{\partial(h(\mathbf{y})\dot{y}_1)}{\partial y_1} + \frac{\partial(h(\mathbf{y})\dot{y}_2)}{\partial y_2} = -c_1 \alpha v y_1(t) \sin y_2(t) < 0.$$

Thus, there is no closed orbit in the region $y_1(t) \in (0, r_d)$ and $y_2(t) \in (0, \pi)$. ■

Proof of Proposition 3: If $\phi(t_0) \in [-\pi, 0]$, it follows from Lemma 13 that the closed-loop system (13) asymptotically converges to $\tilde{\mathbf{x}}_e = [s_e, -\pi/2]'$. Moreover, the convergence speed near $\tilde{\mathbf{x}}_e$ is exponentially fast by Lemma 14. Finally, we show that there is a finite $t_1 > t_0$ such that $\phi(t_1) \in [-\pi, 0]$ for any $\phi(t_0) \in (0, \pi)$, in Lemma 15.

References

- Ai, X., You, K. & Song, S. (2016), A source-seeking strategy for an autonomous underwater vehicle via on-line field estimation, *in* 'International Conference on Control, Automation, Robotics and Vision', IEEE, pp. 1–6.
- Baronov, D. & Baillieul, J. (2007), Reactive exploration through following isolines in a potential field, *in* 'American Control Conference', IEEE, pp. 2141–2146.
- Beard, R. W. & McLain, T. W. (2012), *Small Unmanned Aircraft: Theory and Practice*, Princeton University Press.
- Bourne, J. R., Pardyjak, E. R. & Leang, K. K. (2019), 'Coordinated Bayesian-based bioinspired plume source term estimation and source seeking for mobile robots', *IEEE Transactions on Robotics* **35**(4), 967–986.
- Briñón-Arranz, L., Renzaglia, A. & Schenato, L. (2019), 'Multirobot symmetric formations for gradient and Hessian estimation with application to source seeking', *IEEE Transactions on Robotics* **35**(3), 782–789.
- Cao, Y. (2015), 'UAV circumnavigating an unknown target under a GPS-denied environment with range-only measurements', *Automatica* **55**, 150–158.
- Cochran, J., Siranosian, A., Ghods, N. & Krstic, M. (2009), '3-D source seeking for underactuated vehicles without position measurement', *IEEE Transactions on Robotics* **25**(1), 117–129.
- Deghat, M., Davis, E., See, T., Shames, I., Anderson, B. D. & Yu, C. (2012), Target localization and circumnavigation by a non-holonomic robot, *in* 'IEEE/RSJ International Conference on Intelligent Robots and Systems', IEEE, Vilamoura, pp. 1227–1232.
- Dong, F. & You, K. (2020), 'Coordinate-free isoline tracking in unknown 2-D scalar fields', *submitted to IROS 2020*, see also <https://arxiv.org/pdf/2003.12684.pdf>.
- Dong, F., You, K. & Song, S. (2020), 'Target encirclement with any smooth pattern using range-based measurements', *Automatica*.
- Dong, F., You, K. & Xie, L. (2020), 'Circumnavigating a moving target with range-only measurements', *arXiv:2002.06507*.
- Fonseca, J., Wei, J., Johansson, K. H. & Johansen, T. A. (2019), Cooperative decentralized circumnavigation with application to algal bloom tracking, *in* 'IEEE/RSJ International Conference on Intelligent Robots and Systems', IEEE, Macau, China, pp. 3276–3281.
- Guler, S. & Fidan, B. (2015), Range based target capture and station keeping of nonholonomic vehicles without GPS, *in* 'European Control Conference', pp. 2970–2975.
- Hwang, J., Bose, N. & Fan, S. (2019), 'AUV adaptive sampling methods: A review', *Applied Sciences* **9**(15), 3145.
- Jiang, X. & Li, S. (2018), 'Plume front tracking in unknown environments by estimation and control', *IEEE Transactions on Industrial Informatics* **15**(2), 911–921.
- Joshi, A., Ashley, T., Huang, Y. R. & Bertozzi, A. L. (2009), Experimental validation of cooperative environmental boundary tracking with on-board sensors, *in* 'American Control Conference', IEEE, pp. 2630–2635.

- Kapitanyuk, Y. A., Proskurnikov, A. V. & Cao, M. (2018), ‘A guiding vector-field algorithm for path-following control of nonholonomic mobile robots’, *IEEE Transactions on Control Systems Technology* **26**(4), 1372–1385.
- Khalil, H. K. (2002), *Nonlinear Systems (3rd Ed.)*, Prentice Hall.
- Kim, J.-S., Menon, P. P., Back, J. & Shim, H. (2017), ‘Disturbance observer based boundary tracking for environment monitoring’, *Journal of Electrical Engineering & Technology* **12**(3), 1299–1306.
- Lee, J. (2016), ‘Small fixed wing UAV simulator’.
URL: <https://github.com/magiccjae/ecen674>
- Li, Z., You, K. & Song, S. (2020), ‘Cooperative source seeking via networked multi-vehicle systems’, *Automatica* **115**.
- Lin, J., Song, S., You, K. & Krstic, M. (2017), ‘Stochastic source seeking with forward and angular velocity regulation’, *Automatica* **83**, 378–386.
- Lin, J., Song, S., You, K. & Wu, C. (2016), ‘3-D velocity regulation for nonholonomic source seeking without position measurement’, *IEEE Transactions on Control Systems Technology* **24**(2), 711–718.
- López-Nicolás, G., Aranda, M. & Mezouar, Y. (2020), ‘Adaptive multirobot formation planning to enclose and track a target with motion and visibility constraints’, *IEEE Transactions on Robotics* **36**(1), 142–156.
- Lu, Y. (2017), ‘Quadrotor control, path planning and trajectory optimization’.
URL: <https://github.com/yrlu/quadrotor>
- Malisoff, M., Sizemore, R. & Zhang, F. (2017), ‘Adaptive planar curve tracking control and robustness analysis under state constraints and unknown curvature’, *Automatica* **75**, 133–143.
- Matveev, A. S., Hoy, M. C., Ovchinnikov, K., Anisimov, A. & Savkin, A. V. (2015), ‘Robot navigation for monitoring unsteady environmental boundaries without field gradient estimation’, *Automatica* **62**, 227–235.
- Matveev, A. S., Semakova, A. A. & Savkin, A. V. (2017), ‘Tight circumnavigation of multiple moving targets based on a new method of tracking environmental boundaries’, *Automatica* **79**, 52–60.
- Matveev, A. S., Teimoori, H. & Savkin, A. V. (2011), ‘Range-only measurements based target following for wheeled mobile robots’, *Automatica* **47**(1), 177–184.
- Matveev, A. S., Teimoori, H. & Savkin, A. V. (2012), ‘Method for tracking of environmental level sets by a unicycle-like vehicle’, *Automatica* **48**(9), 2252–2261.
- Mellucci, C., Menon, P. P., Edwards, C. & Challenor, P. (2017), Experimental validation of boundary tracking using the suboptimal sliding mode algorithm, in ‘American Control Conference’, IEEE, pp. 4878–4883.
- Mellucci, C., Menon, P. P., Edwards, C. & Challenor, P. G. (2019), ‘Environmental feature exploration with a single autonomous vehicle’, *IEEE Transactions on Control Systems Technology*.
- Menon, P. P., Edwards, C., Shtessel, Y. B., Ghose, D. & Haywood, J. (2015), Boundary tracking using a sub-optimal sliding mode algorithm, in ‘IEEE Conference on Decision & Control’, pp. 5518–5523.
- Newaz, A. A. R., Jeong, S. & Chong, N. Y. (2018), ‘On-line boundary estimation in partially observable environments using a UAV’, *Journal of Intelligent & Robotic Systems* **90**(3-4), 505–514.
- Strogatz, S. H. (2018), *Nonlinear Dynamics and Chaos: with Applications to Physics, Biology, Chemistry, and Engineering (2nd Edition)*, CRC Press, Boca Raton.
- Swartling, J. O., Shames, I., Johansson, K. H. & Dimarogonas, D. V. (2014), ‘Collective circumnavigation’, *Unmanned Systems* **2**(03), 219–229.
- Wu, W. & Zhang, F. (2012), ‘Robust cooperative exploration with a switching strategy’, *IEEE Transactions on Robotics* **28**(4), 828–839.
- Zhang, F. & Leonard, N. E. (2010), ‘Cooperative filters and control for cooperative exploration’, *IEEE Transactions on Automatic Control* **55**(3), 650–663.
- Zhang, M., Tian, P. & Chen, X. (2017), ‘Unmanned aerial vehicle guidance law for ground target circumnavigation using range-based measurements’, *International Journal of Control Automation & Systems* **15**(5), 2455–2460.
- Zheng, R., Lin, Z., Fu, M. & Sun, D. (2015), ‘Distributed control for uniform circumnavigation of ring-coupled unicycles’, *Automatica* **53**, 23–29.